Experimental Evidence of Hidden Topological Surface States in $PbBi_4Te_7$

Taichi Okuda,[1,*] Takamasa Maegawa,[2] Mao Ye,[1] Kaito Shirai,[2] Takuya Warashina,[2] Koji Miyamoto,[1] Kenta Kuroda,[2] Masashi Arita,[1] Ziya S. Aliev,[3,4] Imamaddin R. Amiraslanov,[3,4] Mahammad B. Babanly,[3] Evgueni V. Chulkov,[5,6,7] Sergey V. Eremeev,[7,8] Akio Kimura,[2] Hirofumi Namatame,[1] and Masaki Taniguchi[1,2]

[1]*Hiroshima Synchrotron Radiation Center (HSRC), Hiroshima University, 2-313 Kagamiyama, Higashi-Hiroshima 739-0046, Japan*
[2]*Graduate School of Science, Hiroshima University, 1-3-1 Kagamiyama, Higashi-Hiroshima 739-8526, Japan*
[3]*General and Inorganic Chemistry Department, Baku State University, AZ1148 Baku, Azerbaijan*
[4]*Institute of Physics, Azerbaijan National Academy of Science, AZ1143 Baku, Azerbaijan*
[5]*Departamento de Fisca de Materiales UPV/EHU, CFM-MPC and Centro Mixto CSIC-UPV/EHU, 20080 San Sebastian/Donostia, Basque Country, Spain*
[6]*Donostia International Physics Center, 20018 San Sebastian/Donostia, Basque Country, Spain*
[7]*Tomsk State University, 634050 Tomsk, Russia*
[8]*Institute of Strength Physics and Materials Science SB RAS, 634021 Tomsk, Russia*

(Received 21 August 2013; published 12 November 2013)

A topological surface state that is protected physically under the Bi_2Te_3-like five-layer block has been revealed on the Pb-based topological insulator (TI) $PbBi_4Te_7$ by bulk sensitive angle-resolved photoelectron spectroscopy (ARPES). Furthermore, conservation of the spin polarization of the hidden topological surface states is directly confirmed by bulk-sensitive spin ARPES observation. This finding paves the way to realize the real spintronics devices by TIs that are operable in the real environment.

DOI: 10.1103/PhysRevLett.111.206803 PACS numbers: 73.20.−r, 71.20.−b, 75.70.Tj, 79.60.−i

Topological insulators (TI) are the new class of quantum matter, possessing topological surface state (TSS) in the bulk energy gap. This state demonstrates spin-polarized massless Dirac cone (DC) behavior with spin orientation of the TSS locked with the crystal momentum and resulting in a helical spin structure. The spin-polarized TSS is protected by the time-reversal symmetry from backscattering by nonmagnetic impurities, is expected to possess the property of dissipationless spin transport, and has attracted much attention because of its potential application to spintonic devices [1–3].

For real applications it is necessary to allocate TSS at the bulk energy band gap and tune the Fermi level at the TSS. In practice, however, surface defects or element substitutions cause the natural doping at the surface and result in the chemical potential shift to bulk continuum states. In fact, the bulk conduction band is quite often observed with TSS below the Fermi level in angle-resolved photoelectron spectroscopy (ARPES), and many efforts to tune the Fermi level in the bulk band gap by electron or hole doping in the crystal growth [4,5] or alkali metal or NO_2 adsorption at the surfaces [6] have been made so far. Only in few of these, however, has the contribution of TSS been clearly observed in the transport measurement [7].

Even though the Fermi-level tuning was successful, it has been reported that the small amount of adsorption of residual gas or water easily causes the energy shift of the TSS [6,8] and casts away the efforts of the carrier control. Therefore, not only the protection by the time-reversal symmetry but some physical protection of the TSS must be necessary for practical applications.

In this Letter, we have demonstrated that the layered Pb-based topological insulator, $PbBi_4Te_7$, can be a promising TI for the practical application. Direct evidence of the physically protected TSS that is well below the Bi_2Te_3-like five-layer block is clearly observed by the bulk-sensitive ARPES measurement. Further, conservation of the spin polarization of the buried TSS is also directly confirmed by the bulk-sensitive spin-resolved ARPES measurement. In addition, scanning tunneling microscopy observation consolidates the results obtained by the photoemission measurements.

High-resolution ARPES and spin ARPES measurements have been done at beam line BL-9A and 9B of Hiroshima Synchrotron Radiation Center (HiSOR). Samples are fabricated by Bridgman method, and the clean surface was obtained by cleavage in the ultrahigh vacuum ($\sim 10^{-9}$ Pa order). High-resolution ARPES spectra have been taken by the VG Scienta R4000 analyzer with Xe discharge lamp at BL-9A, while the spin ARPES spectra were obtained with Xe lamp and 22 eV synchrotron radiation (SR) light at the ESPRESSO end station at BL-9B [9]. At the end station, the surface-sensitive normal ARPES measurement has also been done with SR light. Scanning tunneling microscopy (STM) and spectroscopy (STS) have been done with a low-temperature STM system (Omicron GmBH) at the sample temperature of about 80 K.

The electronic structure calculations were performed within the density functional theory implemented in VASP code [10,11] with the van der Waals nonlocal correlation functional include (see [12] for more details).

Figure 1(a) shows the atomic structure of $PbBi_4Te_7$ which consists of the alternate stacking of five-layer block (Te-Bi-Te-Bi-Te) and seven-layer block (Te-Bi-Te-Pb-Te-Bi-Te). These blocks correspond to the Bi_2Te_3 and $PbBi_2Te_4$ structures, respectively. The two blocks are weakly bonded to each other by the van der Waals interaction and the crystal tends to cleave at the van der Waals gap. Therefore, there are two possible terminations of the topmost surface, i.e., five-layer block (5LB) and seven-layer block (7LB) termination. The slab calculations presented in Fig. 1 were performed using the following symmetric slabs: 41 and 43 atomic layer slabs where the upper and lower surfaces have identical termination (5LB and 7LB, respectively) as well as asymmetric slab of 48 atomic layers where opposite surfaces have different termination. The latter was done to find out the exact relative positions of the Dirac points (DP) on different surface terminations. As one can see in Fig. 1(b), both surface terminations hold spin-polarized Dirac surface states with clockwise spin helicity. The DP of the 5LB-terminated surface was found 53 meV below the DP of the 7LB-terminated surface. In accordance with earlier predictions [13,14], the spatial distribution of the charge density of TSS is different between 5LB- and 7LB-terminated surfaces [Fig. 1(c)]. Namely, at the 7LB-terminated surface the charge density of TSS is predominantly distributed within the topmost 7LB, while in the case of the 5LB-terminated surface, the TSS is distributed well below the first 5LB and mostly located at the subsurface 7LB.

In order to study the depth profile of the TSS, we have applied ARPES measurement with different surface sensitivities using two different photon energies from a Xe discharge lamp ($h\nu = 8.4$ eV) and SR ($h\nu = 22$ eV). According to the universal curve of the electron mean-free path, the resulting kinetic energy of ~4 and ~18 eV by the Xe and the SR excitation provides a large difference of the mean-free path of electrons of ~100 Å and ~5 Å [15]. Thus, one can in principle do depth-dependent ARPES observation using these light sources, although the photoemission intensity is also affected by the photoexcitation transition matrix element in this energy region.

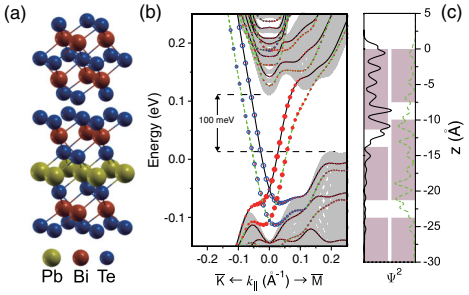

FIG. 1 (color online). (a) Crystal structure of $PbBi_4Te_7$. (b) Calculated band structure of $PbBi_4Te_7(0001)$ with seven- and five-layer block termination (black solid and green dashed curves, respectively); circles represent weights of the states in the two outermost blocks multiplied by value of in-plane spin components (red (filled circles) and blue (open circles) denote positive and negative values of spin, respectively). Shaded area is the bulk-projected bands, and the bulk band gap is about 100 meV. (c) Depth profile of the charge density of the topological surface state for 5LB- (green dashed line) and 7LB-terminated (black solid line) surface.

Figures 2(a) and 2(b) are the observed electronic band structures of $PbBi_4Te_7$ by SR and Xe excitation, respectively. In order to see clearly the band dispersion, the second derivatives of Figs. 2(a) and 2(b) are also presented in Figs. 2(c) and 2(d). As in Fig. 2(a) one can observe only a single DC in the surface-sensitive ARPES data taken with SR excitation. Although the DP is not clearly observed in this photon energy, almost straight DC-like dispersion can be seen both in the $\bar{\Gamma}$-$\bar{M}$ and $\bar{\Gamma}$-$\bar{K}$ direction.

In contrast, in the bulk sensitive ARPES data taken with the Xe excitation, much richer structures are observed, as shown in Figs. 2(b) and 2(d). With this photon energy, we can much more clearly observe the DC, and the DP can be estimated as about $E_B = 0.39$ eV from the Fermi level. The band structure of the upper DC is not linear, but kinklike structures have been observed at around $E_B = 0.3$ and 0.1 eV, especially in $\bar{\Gamma}$-$\bar{M}$ direction. This kinklike band dispersion is not clear in the $\bar{\Gamma}$-$\bar{K}$ direction, suggesting that the characteristic band structure is due to the warping effect [16]. Comparing the dispersions, the characteristics of the band structure of DC observed by Xe excitation (we call it DC1 hereafter) are in good agreement with the ones observed by SR excitation (DC1' hereafter) in both the $\bar{\Gamma}$-$\bar{M}$ and $\bar{\Gamma}$-$\bar{K}$ directions. Although the energy of DP of DC1' cannot be estimated directly because of the lack of the intensity around DP, by assuming the linear dispersion, the DP can be roughly estimated as $E_B = 0.39$–0.40 eV, in fair agreement with the one estimated from the dispersion of DC1 in Fig. 2(b). These coincidences of the dispersion and binding energy of DP suggest that the DC1 and DC1' are the same TSS.

Very interestingly, one more DC-like structure has been observed on the outer side of the DC1 in the bulk sensitive ARPES data. Note that this second DC-like structure (DC2) is completely absent in the surface-sensitive ARPES data in Figs. 2(a) and 2(c). In the $\bar{\Gamma}$-$\bar{M}$ direction, the DC2 seems to merge into the DC1 at around $E_B = 0.25$ eV, while in $\bar{\Gamma}$-$\bar{K}$ it can be observed continuously until the Fermi level.

The absence of the DC2 band in the surface-sensitive ARPES measurement invokes the predicted charge distribution of the 5LB-terminated surface in the $PbBi_4Te_7$ in which the charge density of DC is far beneath the 5LB and located at 7LB subsurface under the 5LB [see Fig. 1(c)]. Thus, the DC2 observed only in the bulk sensitive measurement can be interpreted as the buried TSS on the 5LB-terminated surface. In both directions the DC2 is merged into the bulk band at around $E_B = 0.4$ eV, and the DP cannot be estimated directly. We have roughly

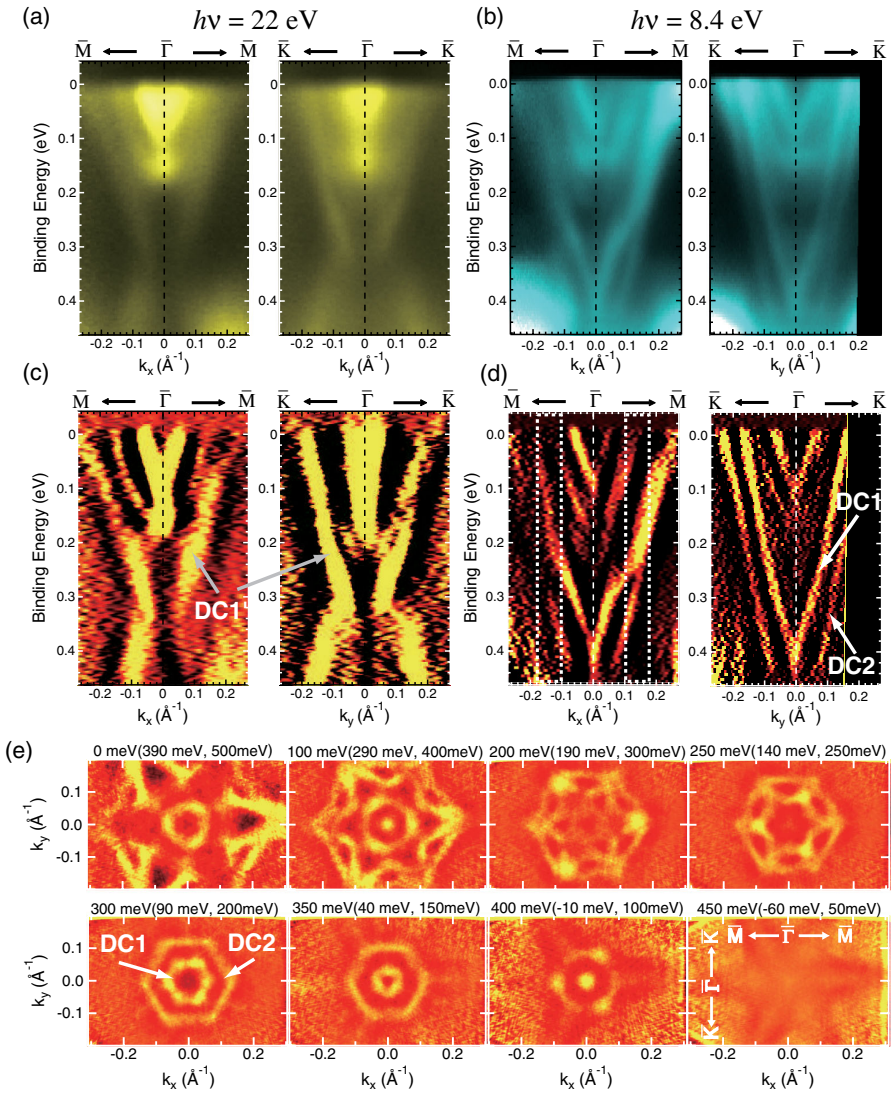

FIG. 2 (color online). Band dispersion of $PbBi_4Te_7$ along $\bar{\Gamma}$-$\bar{M}$ and $\bar{\Gamma}$-$\bar{K}$ directions observed with (a) surface-sensitive ARPES measurement with SR excitation ($h\nu = 22$ eV) and (b) bulk-sensitive ARPES measurement with Xe excitation ($h\nu = 8.4$ eV). The second derivative images of both (a) and (b) are also presented in (c) and (d). (e) Iso-energy contour (IEC) plots of the band dispersion of $PbBi_4Te_7$ taken with Xe excitation. The patterns are second derivative of the raw data with threefold symmetrization. Energies indicated on each IEC are binding energy (left), estimated energy from the DP of DC1 (middle), and DC2 (right), respectively.

estimated the DP as about $E_B = 0.5$ eV by the extrapolation of the observed dispersion in Fig. 2(d).

In order to investigate the strength of the warping effect, the iso-energy contour (IEC) of the band structure was obtained with Xe excitation in Fig. 2(e). In each IEC, binding energy and the energy from the estimated DP of DC1 and DC2 are indicated. Near the DP (at $E_B =$ 400 meV), DC1 shows circlelike IEC and the shape changes to the hexagon at E_B=300 meV (+90 meV from DP). After that it changes to a snowflakelike shape above $E_B = 250$ meV (+ 140 meV from DP) by the warping effect. On the other hand, DC2 shows much weaker warping than DC1 and even quite far beyond the DP, the shape is still hexagonal. If the hypothesis that the DC1 and DC2 are the TSS of 7LB- and 5LB-terminated surfaces is correct, this tendency is in good agreement with that obtained from the previous calculation [14] and present calculation, which show larger warping on the 7LB-terminated surface than on the 5LB-terminated surface (see [17] for more information).

To verify if the observed DC-like structures (DC1, DC1', and DC2) are spin polarized, spin ARPES measurement has been done. For the observation of DC1(DC1'), we have utilized surface-sensitive conditions in which we can selectively observe only the DC1(DC1') state. In Fig. 3(a), a series of spin ARPES data taken with SR excitation ($h\nu =$ 22 eV) is presented. Linear dispersion with spin polarization which is reversed with respect to the $\bar{\Gamma}$ point is clearly observed. The spin polarization inversion is apparent in the spin polarization map in Fig. 3(a), strongly supporting that

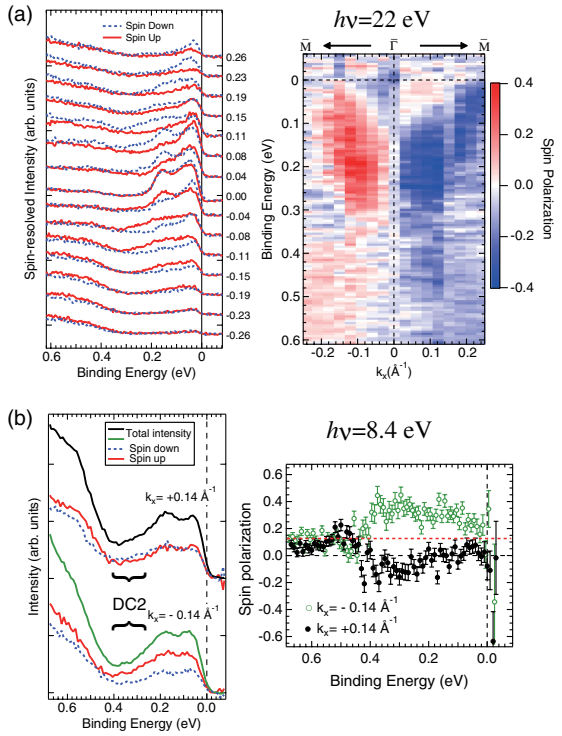

FIG. 3 (color online). (a) Surface-sensitive spin ARPES spectra and polarization map taken with SR excitation ($h\nu = 22$ eV). (b) Bulk-sensitive spin ARPES spectra and polarization spectra obtained with Xe excitation at $k_x = \pm 0.14$ Å^{-1}. The measurement positions of the data are indicated with the rectangles in Fig. 2(d). The width of the rectangles indicates the angular resolution of the measurement.

the observed DC1(DC1') state is TSS of $PbBi_4Te_7$. Note that the spin polarization observed near the Fermi level at the Brillouin zone center is most likely due to the Rashba-like spin splitting caused by the aging effect [18,19].

For the observation of the DC2 state we have utilized bulk-sensitive conditions with Xe excitation. The spin ARPES spectra and its spin polarization of DC2 are presented in Fig. 3(b). Since the signal of DC2 by the bulk-sensitive spin ARPES is relatively weaker, we took the data at only two points in k space ($k_x = \pm 0.14$ Å^{-1}), which are indicated in Fig. 2(d) by dashed rectangles. As in Fig. 3(b), at $k_x = 0.14$ Å^{-1} the spin polarization of DC2 at around $E_B \sim 0.25$–0.4 eV is slightly dominated by the spin-down state. In contrast, at $k_x = -0.14$ Å^{-1} the spin-up state is largely dominating the DC2 state. The difference of the spin polarization between $k_x = +0.14$ Å^{-1} and $k_x = -0.14$ Å^{-1} is much more clearly seen in the spin-polarization spectra in the right panel of Fig. 3(b) in which almost mirror-symmetric behavior against the (red-)dotted line is observed. The results suggest that the spin polarization of DC2 is opposite between positive and negative k values in the initial state but getting some offset spin polarization probably due to the spin-dependent matrix element effect, as discussed in the previous study [20]. Considering this offset spin polarization, the spin polarization of DC2 is reversed with respect to the $\bar{\Gamma}$ point, suggesting that the DC2 is another TSS of $PbBi_4Te_7$, which revealed by the bulk-sensitive ARPES observation. Note that the sign of the spin polarization of DC2 is the same as that of the DC1, and both DC1 and DC2 have clockwise helical spin structure, in good agreement with the calculations [see Fig. 1(b)].

To further elucidate the photoemission results, we have performed STM and STS observation of the sample. Figures 4(a) and 4(b) are the topographic and dI/dV images of $PbBi_4Te_7$ in large scale (500×500 nm^2), and 4(c) is the height profile along the line in Fig. 4(a). As in the figure, there are two kinds of steps with different step height. One is about 1.5 nm high and the other is about 1.0 nm high, and they are lining alternatively. These step heights are in good agreement with that of the 7LB and 5LB of the $PbBi_4Te_7$. As in the dI/dV image, the terrace with 7LB termination shows darker contrast than that with 5LB termination, indicating that the differently terminated terrace has different surface electronic structure.

In Figs. 4(d) and 4(e) high-resolution images of 5LB- and 7LB-terminated surfaces are presented. The 7LB-terminated surface resembles the atomic image of $PbBi_2Te_4$ (see inset), while the image of the 5LB-terminated surface is almost identical to that of the Bi_2Te_3 [21], consistent with the crystal structure of the sample [see Fig. 1(a)].

As in Fig. 4(f) the observed STS spectra are strikingly different between the terraces of 7LB and 5LB termination. In the 7LB termination, one can see clearly the dip

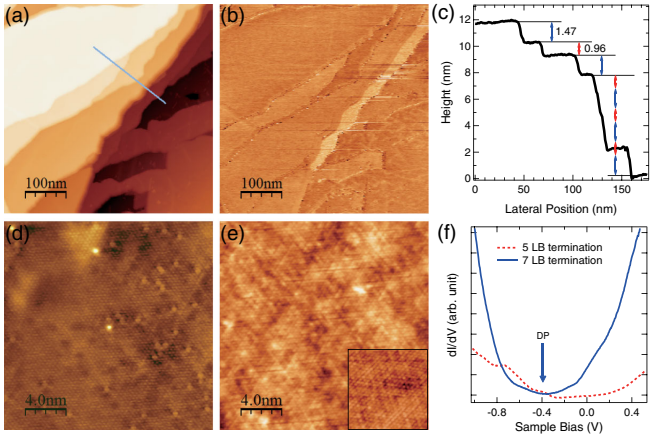

FIG. 4 (color online). (a) STM topographic image and (b) dI/dV image of $PbBi_4Te_7$ taken at Vs $= -0.6$ V. (c) The height profile along the line in (a). Two kinds of steps with different step height that correspond to 7 LB and 5 LB are clearly seen. Atomic resolution dI/dV images are obtained at Vs $= -0.1$ V on the terrace of (d) 5LB and (e) 7LB termination, respectively. Image of $PbBi_2Te_4$ in the same scale is also indicated in the inset of (e). (f) STS spectra taken at the different terraces. On the 7LB termination, DP is observed at around -0.39 V. While on the 5LB termination, no clear evidence of DC is observed.

structure that corresponds to the drop of the density of states at the DP. The energy of the dip position (~ -0.39 eV) is in good corresponding to the DP energy observed by ARPES. In the case of the 5LB-terminated terrace, however, the dip structure is not clear and the existence of DC is not evident. The lack of the DC properties in STS on the 5LB-terminated surface supports the interpretation that the DC2 observed by the bulk-sensitive ARPES measurement is the electronic structure of TSS that is located in the 7LB subsurface and buried under the 5LB, i.e., physically protected TSS.

A different interpretation has been reported previously on $PbBi_4Te_7$ [14]. From the ARPES and spin ARPES measurements with the photon energy of $h\nu = 21$ eV, as well as the STM observation, Eremeev *et al.* concluded that the surface defects destroy the surface electronic structure of the sample and only the electronic structure of the 7LB, which is under the 5LB, can be observed with their photoemission measurement. However, the annihilation of the TSS by surface defect is not likely judging from the clear STM image with atomic resolution in their study. The interpretation is mainly derived from their IEC measurement in which a highly warped snowflake pattern expected for the 7LB termination is absent, and only the hexagonal shape from the moderate warping effect expected for the 5LB termination is observed at 100 meV above DP. As shown in Fig. 2(e), in the present measurement the clear snowflake pattern can be seen at energies higher than 250 meV from the DP of DC1 (DC1'), and the warping effect is a little weaker than the expectation by the previous calculation. Indeed, taking the van der Waals interaction into account, calculation leads to substantially weaker warping for the 7LB termination (Fig. S2 [17]). Hence, the IEC observed by the previous study is probably from the topmost surface of the 7LB termination, while the DC underneath the 5LB terminated terrace is not observed in their surface-sensitive ARPES condition.

In conclusion, the electronic structure of Pb-based layered ternary telluride $PbBi_4Te_7$ has been investigated by depth-selective ARPES and spin ARPES measurements as well as by the STM and STS observations. In addition to the TSS in the 7LB-terminated terrace, another TSS that is at the 7LB subsurface and buried under the 5LB has been revealed by the bulk-sensitive ARPES. Furthermore, the conservation of the spin polarization under the 5LB is directly confirmed by bulk-sensitive spin ARPES measurement. The finding of the well-protected spin-polarized TSS under the thick protecting layer opens a new pathway for the application of the topological insulator to the real spintronic devices in the future.

This work was partly supported by KAKENHI (No. 19340078, No. 23244066 and No. 23340105) Grant-in-Aid for Scientific Research (B) and (A) of Japan Society for the Promotion of Science. The experiments were performed with the approval of the Proposal Assessing Committee of the Hiroshima Synchrotron Radiation Center (Proposal No. 12A-25). For the analysis of STM data free software WSxM [22] was used.

*okudat@hiroshima-u.ac.jp

[1] M. Z. Hasan and C. L. Kane, Rev. Mod. Phys. **82**, 3045 (2010).
[2] X.-L. Qi and S.-C. Zhang, Rev. Mod. Phys. **83**, 1057 (2011).
[3] Y. Ando, J. Phys. Soc. Jpn. **82**, 102001 (2013).
[4] D. Hsieh, Y. Xia, D. Qian, L. Wray, J. H. Dil, F. Meier, J. Osterwalder, L. Patthey, J. G. Checkelsky, N. P. Ong, V. Fedorov, H. Lin, A. Bansil, D. Grauer, Y. S. Hor, R. J. Cava, and M. Z. Hasan, Nature (London) **460**, 1101 (2009).
[5] S. Jia, H. Ji, E. Climent-Pascual, M. K. Fuccillo, M. E. Charles, J. Xiong, N. P. Ong, and R. J. Cava, Phys. Rev. B **84**, 235206 (2011).
[6] S. Xu *et al.*, Science **332**, 560 (2011).
[7] Z. Ren, A. A. Taskin, S. Sasaki, K. Segawa, and Y. Ando, Phys. Rev. B **82**, 241306 (2010).
[8] P. D. C. King *et al.*, Phys. Rev. Lett. **107**, 096802 (2011).
[9] T. Okuda, K. Miyamaoto, H. Miyahara, K. Kuroda, A. Kimura, H. Namatame, and M. Taniguchi, Rev. Sci. Instrum. **82**, 103302 (2011).
[10] G. Kresse and J. Hafner, Phys. Rev. B **48**, 13 115 (1993).
[11] G. Kresse and J. Furthmüller, Comput. Mater. Sci. **6**, 15 (1996).
[12] See Supplemental Material at http://link.aps.org/supplemental/10.1103/PhysRevLett.111.206803 for detailed information on the calculation.
[13] S. V. Eremeev, Y. M. Koroteev, and E. V. Chulkov, JETP Lett. **92**, 161 (2010).
[14] S. V. Eremeev *et al.*, Nat. Commun. **3**, 635 (2012).
[15] M. P. Seah and W. A. Deuch, Surf. Interface Anal. **1**, 2 (1979).
[16] L. Fu, Phys. Rev. Lett. **103**, 266801 (2009).
[17] See Supplemental Material at http://link.aps.org/supplemental/10.1103/PhysRevLett.111.206803 for the quantitative comparison of the warping effect.
[18] M. Bianchi, R. C. Hatch, J. Mi, B. B. Iversen, and P. Hofmann, Phys. Rev. Lett. **107**, 086802 (2011).
[19] S. V. Eremeev, M. G. Vergniory, T. V. Menshchikova, A. A. Shaposhnikov, and E. V. Chulkov, New J. Phys. **14**, 113030 (2012).
[20] C. Jozwiak, Y. L. Chen, A. V. Fedorov, J. G. Analytis, C. R. Rotundu, A. K. Schmid, J. D. Denlinger, Y. D. Chuang, D. H. Lee, I. R. Fisher, R. J. Birgeneau, Z. X. Shen, Z. Hussain, and A. Lanzara, Phys. Rev. B **84**, 165113 (2011).
[21] G. Wang, X.-G. Zhu, Y.-Y. Sun, Y.-Y. Li, T. Zhang, J. Wen, X. Chen, K. He, L.-L. Wang, X.-C. Ma, J.-F. Jia, S. B. Zhang, and Q.-K. Xue, Adv. Mater. **23**, 2929 (2011).
[22] I. Horcas, R. Fernandez, J. M. Gomez-Rodriguez, J. Colchero, J. Gomez-Herrero, and A. M. Baro, Rev. Sci. Instrum. **78**, 013705 (2007); see also Nanotec Electronica at http://www.nanotec.es.